International Research Journal of Engineering and Technology (IRJET) e-ISSN: 2395-0056
Volume: 11 Issue: 03 | Mar 2024 www.irjet.net p-ISSN: 2395-0072

Response surface statistical optimization of photocatalytic degradation of RO86 dye using Fe-N-TiO_2

Srujana Dhegam[1], Sailu Chintha[2], Hari babu Pengonda[3], Jyothi Thati[4]

[1,3]ph.D scholar, Dept. of Chemical Engineering, University College of Technology, Osmania University, Telangana, India
[2] Professor, Dept. of Chemical Engineering, University College of Technology, Osmania University, Telangana, India
[4]Associate professor Dept. of Chemical Engineering, University College of Technology, Osmania University, Telangana, India.

Abstract - *Textile production units are the foremost economic industrial zones prevailing across the globe but produce enormous amounts of wastewater which confines to high levels of chemicals and pollutants during their processing stages. To eradicate these pollutants an attempt is made by using advanced oxidation processes and solar energy. In this context, the present study includes utilization of solar energy by altering the optical Titanium dioxide (TiO_2) by doping and Co-doping with Nitrogen (N), Iron (Fe). Synthesized catalysts were characterized by X-ray diffraction (XRD) Scanning Electronic Microscopy (SEM), Fourier transform infrared spectrophotometer (FTIR) & UV–Vis Diffuse Reflectance Spectra (UV–Vis DRS). Based on XRD patterns, the average crystallite size was determined using Debye-Sherrer, Williamson -Hall (W-H) and Halder-Wagner (H-W) methods. SEM explored the shape of catalyst by increasing the Fe content. Functional groups were identified in between 500 cm-1- 3600 cm-1. UV- Vis DRS analyzed the band gap of Fe-N-TiO_2 (2.8eV) is lesser than that of N-TiO2 (3.1eV). By selecting Fe-N-TiO_2_1 as a photocatalyst, the percentage degradation of RO86 dye under solar light was determined by Design of Experiments-Response Surface Methodology-Central Composite Design (DOE-RSM-CCD). Optimum conditions for maximum degradation of 97.39% of Reactive Orange-86(RO-86) were achieved with a catalyst dosage of 1.388 g/250 ml, 10 mg/l concentration, reaction time of 148 min and rate constant 0.0158min-1 with first order reaction.*

Key Words: Advanced Oxidation Process, Reactive Orange-86, Response Surface Methodology, degradation

1. INTRODUCTION

In the present era, water pollution is a significant issue caused by the major contribution of industrial civilization. Treating the effluents before entering water bodies is the key challenge for the various industries like paper, textile, pulp, and metallic industries etc. Amongst all, textile industries are key corners of extensively discharging effluents in water bodies in the downstream processing units such as dyeing and finishing [1]. Effluents evolved from dyeing and rinsing units show endangered environmental impacts as it carries over much colour and is exceptionally conductive because of existence of substantial presence of free dye molecules [2]. Reactive dyes are significantly employed in dyeing operations to impart colour on fabrics for of their distinct reactivity and better colour longevity [3]. As the Reactive dyes are remarkably miscible with water, malignity & recalcitrancy parameters leads to serious carcinogenic diseases [4]. There exist numerous conventional methods to decolorize the textile effluents such as adsorption (using various adsorbents), electrochemical treatment, coagulation / flocculation, ozonation, biological & chemical oxidation [5]. However, these methods have inherent and distinct disadvantages in terms of feasibility of operation and cost of the technique employed towards complete degradation of dyes [6].

To overcome this, Advanced Oxidation Process (AOP's) are set as cutting-edge technologies for treating dye effluents. AOPs rely on development of extremely reactive species like OH. to initiate oxidation of pollutant molecules which can be produced at near ambient pressure and temperature. AOP can significantly degrade the organic pollutants to CO_2, H_2O and salts [7]. From the diversified AOPs, heterogeneous photocatalysis is preferred choice for the degradation of stable dye complex structures [8]. In heterogeneous photocatalysis, the predominant factor is figuring out the reliable catalyst. TiO_2 is the most abundantly used catalyst for photo-catalyzed reactions by virtue of its properties like electronic configuration, optical band gap (3.2eV), occurrence, thermal stability, chemical resistant and non-poisonous [9]. In spite of this, TiO_2 is suffering with two shortcomings like; it requires excess energy like UV radiation to excitation of electronics from VB to CB and rapid recombination of e^- -h^+ pairs [10]. On the other hand, solar radiation comprises 4-5% of Ultraviolet radiation. With a view to utilize the remaining portion of sunlight radiation like visible region, it is necessary to cut-down the band gap by employing most promising methods like doping [11].

Doping can alter the optical response by creating new energy levels in between VB and CB [12]. However, doping with non-metals like N, C, and S is the most fashionable. But doping with Nitrogen (N-TiO_2) is more effective which can shift absorption band spectra from UV to visible light [13]. Though N-TiO_2 can absorb visible light spectra of solar

radiation [14], the photocatalytic activity was not complete, because doping with N (wt %) leads to TiO_2 lattice distortion with increase in e^--h^+ recombination rate by localization of N2p states [15] [16]. To surpass this, many researchers suggested metal & non-metal co-doping of TiO_2 [17]. Co-doping of N-TiO_2 with Fe would dial down recombination rate effectively. Even a minimal amount of Fe+3 ions can act as a trapping centre to inhibit electron-hole recombination [16]. This study focused attention on the degradation of Reactive Orange 86 (RO86) dye as depicted in fig.1 using Fe-N-TiO_2_1as a photocatalyst under visible radiation by optimization of various parameters of the dye solution like catalyst dosage, the concentration of RO86, and time of reaction. The investigation of the influence of individuals and the interaction of parameters on the degradation of dye is carried out by using Response Surface Methodology (RSM). RSM is a powerful statistical tool to establish the design of experiments (DOE) involving several variables [18]. In this work, The Central Composite Design (CCD) based RSM was adopted to analyse the system with 3 parameters on 2 levels (23).

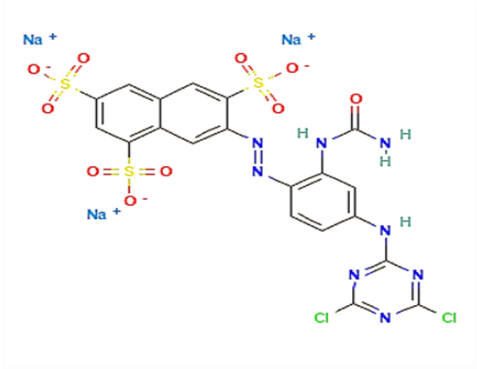

Fig.1 Chemical structure of a commercial Reactive Orange-86 dye (λ=412nm) running text should match with the list of references at the end of the paper.

2. METHODS

2.1 Reagents and Chemicals

Titanium Tetra Isopropoxide (TTIP) was purchased from Sigma-Aldrich, Iron (III) Nitrate nano hydrate $Fe(NO_3)_3.9H_2O$, Urea (NH_2CONH_2) were brought from Isochem and Glacial Acetic Acid, Absolute Ethanol (99.9%), Double distilled water (DDW) of analytical grade were directly utilized and Reactive Orange-86 dye ($C_{20}H_{11}Cl_2N_8Na_3O_{10}S_3$)) (M.W. = 759.4 gmol−1) used for degradation studies.

2.2 Synthesis of N-TiO_2 Photocatalyst

2.2.1 Solution A

Solution A is prepared by adding titanium tetra iso propoxide (TTIP) (10 ml) to 30 ml of absolute ethanol under constant mixing for 1hr.

2.2.2 Solution B

Solution B is prepared by adding different amounts of urea (0.3 and 0.6g) in 50 ml of DDW and 1 ml of glacial acetic acid under constant stirring for 30min which acts as a precursor for the Nitrogen source.

Add solution B drop-wise to solution A under brisk mixing for 1hr at room temperature. The resultant precipitate was kept for aging for 12hrs and later dried at 120°C for two hours. Obtained sample was calcinated in a muffle furnace for about 1hr at 400°C with a heating rate of 4°C/min [19].

2.3 Synthesis of Fe- N-TiO_2 Photocatalyst

2.3.1 Solution B

Solution B is prepared by adding different amounts of 0.02g and 0.04g of Nitrate Nano hydrate (Fe(NO3)3.9H2O) which acts as a precursor for Iron source, 0.3g of urea in 50 ml of DDW and 1ml of glacial acetic-acid and under constant stirring for 30min. Then the remaining procedure was the same after adding this solution drop-wise solution A.

2.4 Catalyst Characterization

X-ray diffraction (XRD) results of synthesized crystalline structures reported in this study were studied on a Rigaku X-Ray Diffractometer by using Ni-filtered Cu Kα radiation (λ = 1.5406 Ao) in the range of 10°< 2θ <80° with a step size of 0.02°/2θ under operating with 40 kV and 30 mA accelerating voltage and current respectively. Scanning electron microscopy (SEM) (JSM-7800F) was used to study morphology and chemical compositions, Japan, FTIR (Fourier transform infrared spectrophotometer) (Model FTIR-8400S, SHIMADZU) were utilized to identify functional groups presented in. UV-Vis Diffuses Reluctance (UV-Vis DRS) Spectra (Hitachi U-3900 spectrometer), using the reference ($BaSO_4$ standard) in the range of 200-1000 nm.

2.5 Photocatalytic Experiments

250 ml of RO86 dye solution (10, 55, and 100 mg/l) in a batch reactor were taken for the below experimentation. The experiments were conducted using solar light with the required amount of catalyst (0.5, 1, and 1.5 gm) under constant vigorous stirring of the solution at 400 rpm. Dye samples were stored in the dark to attain the equilibrium between the dye solution and catalyst particle at the beginning. An aliquot of 10 ml was collected at 30 and 180 min and filtered via Millipore-filter (0.45 µm) and was further analyzed using UV-Visible Spectrophotometer (Shimadzu, model UV-1800). The % of degradation of the dye solution was determined as follows:

$$\%Degradation = \frac{A_0 - A}{A_0} \times 100$$

Where A_0 and A are the initial and final absorbance values of samples at any time respectively.

2.5.1Design of Experiments using Response Surface Methodology (RSM)

RSM approach is used to depict effects of various independent factors on process response. RSM is used to minimize the number of experiments and to analyze the experimental design results with the predicted results. Catalyst dosage, concentration (RO86), and time of reaction on degradation performance were investigated. Central Composite Design (CCD) at two levels involving three parameters [20] as shown in Table-1.

Table-1: Operating levels of independent factors in RSM-CCD.

S. No.	Independent factor	Low level (-1)	High level (+1)
1.	Catalyst dosage(g)	0.5	1.5
2.	Concentration(mg/l)	10	100
3.	Time of reaction(min)	30	180

By operating the process at 2 levels with 3 parameters ($2^k=2^3$) factorial design generated 20. Experiments by using the RSM-CCD method were shown in Table 2. Catalyst dosages were in the range of 0.5-1.5 g/250 ml, the concentration of dye solution was in the range of 10-100mg/l, and the reaction time varied from 30-180 min. These independent variables were designated as X_1, X_2, and X_3 respectively. Degradation efficiency response was estimated to investigate the process variables.

To get a good estimate of experimental errors during experimental analysis five replications conducted [21].

A quadratic model was developed to support the experimental validation shown as below:

$$Y=b_0 + b_1X_1 + b_2X_2 + b_3X_3 + b_{11}X_1^2 + b_{22}X_2^2 + b_{33}X_3^2 + b_{12}X_1X_2 + b_{13}X_1X_3 + b_{23}X_2X_3$$

Where, Y: Predicted response factor of % degradation RO86, b_0: Constant coefficient, b_{11}, b_{22} and b_{33}: quadratic coefficients, b_{12}, b_{13} and b_{23}: Interaction coefficients respectively. X_1, X_2, and X_3 have coded forms of parameters [22]

2.6 Reaction Kinetics

To enhance the rate of mass transfer of dye molecules to the photocatalyst surface were maintained with sufficient mixing of slurry during each batch period. The photocatalytic reaction rate was modeled with first order on degradation as following [22]:

$$\frac{dA}{dt} = R_D$$

R_D is the rate of degradation of dye molecules with first-order reaction which is represented as follows:

$$ln\frac{A_0}{A} = kt$$

Where A is the absorbance of samples collected at various reaction time, A_0 is the initial absorbance value, k is the rate constant of first order reaction(min^{-1}) and t is the reaction time(time).

3. RESULTS & DISCUSSIONS

3.1XRD Patterns

To evaluate the effect of doping elements (Fe, N) on TiO_2 crystal structure XRD patterns of four catalyst compositions were recorded as shown in Fig. 2.

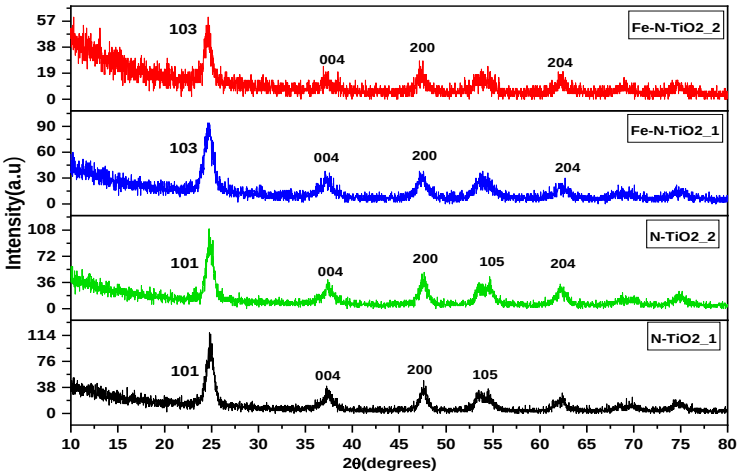

Fig. 2: XRD Patterns of all synthesized catalyst samples

The XRD patterns are consensus with identical crystal structures (01-081-1387, 01-071-1169). All these four types of photocatalysts are tetragonal (BCC) and anatase phases accounting for most diverse distinct diffraction peaks corresponding to the (101), (004), (200), (103), (105), (211), and (204) crystal planes.

Debye–Scherer (DS) Equation as mentioned below is used for calculating the average crystallite size

$$\frac{K\lambda}{\beta cos\theta}$$

Where '*D*' is the average crystallite size, '*k*' is the grain-shape-dependent constant (0.9), '*λ*' is the wavelength of X-rays used, 1.5406 Å, '*β*' is the full-width half maximum (FWHM) and '*θ*' is the Bragg's angle of the corresponding peak, respectively [23]. The results obtained were shown in Table 3. The average crystallite size decreased from N-TiO_2_1 to Fe-N-TiO_2_1 and increased from Fe-N-TiO_2_1 to Fe-N-TiO_2_2 indicating the initial decrease in size from N-TiO_2_1 to N-TiO_2_2 is due to replacement of a greater number of oxygen ions with nitrogen ions and further decrease results in replace of Ti^{+4} with Fe^{+3}.

Table-2: Factorial design

Run No.	Catalyst dosage(mg)	Factors		Run No.	Catalyst dosage(mg)	Factors	
		Concentration (mg/l)	Reaction time (min)			Concentration (mg/l)	Reaction time (min)
1	0.5	10	30	11	1	10	105
2	1.5	10	30	12	1	100	105
3	0.5	100	30	13	1	55	30
4	1.5	100	30	14	1	55	180
5	0.5	10	180	15	1	55	105
6	1.5	10	180	16	1	55	105
7	0.5	100	180	17	1	55	105
8	1.5	100	180	18	1	55	105
9	0.5	55	105	19	1	55	105
10	1.5	55	105	20	1	55	105

The result from Fe-N-TiO_2_1 to Fe-N-TiO_2_2 indicates an increase in the concentration of Iron leads to replace of more Ti^{+4} with Fe^{+3} and some of Fe^{+3} is placed interstitially in the lattice which leads to an increase the in volume of the crystal. By using Bragg's law, the lattice parameters of different samples are determined shown in Table 3.

Table-3: Average crystallite size for different types of catalysts with lattice parameters

Type of Catalyst	Avg. Crystallite size (D, nm)	a (A°)	b (A°)	c (A°)
N-TiO_2_1	11.11773	3.829	3.829	9.607
N-TiO_2_2	10.133	3.823	3.823	9.57
Fe-N-TiO_2_1	9.435712	3.879	3.879	10.58
Fe-N-TiO_2_2	10.39278	3.877	3.877	10.56

3.1.1 Dependence of peak broadening

Williamson and Hall (W-H) and Halder-Wagner (H-W) plots are carried out as shown in Fig. 4 to distinguish the crystallite size–affect broadening and intrinsic strain–affect broadening.

3.1.2 Williamson and Hall (W-H) plot method

Williamson and Hall (W-H) plot method relates the XRDpeak broadening by tiny crystallite size and intrinsic strain (ε_S) which is shown as [24]

$$\beta_{hkl} = \beta_D + \beta_S = \frac{K\lambda}{Dcos\theta} + 4\varepsilon_S tan\theta \ldots\ldots (1)$$

by multiplying the above equation (1) by cosθ leads to

$$\beta_{hkl} cos\theta = \frac{K\lambda}{D} + 4\varepsilon_S sin\theta \ldots\ldots (2)$$

by plotting β_{hkl} cosθ on Y-axis and 4sinθ on X-axis provides slope which is the intrinsic strain (ε_s) and intercept (Kλ)/D gives crystallite size (D).

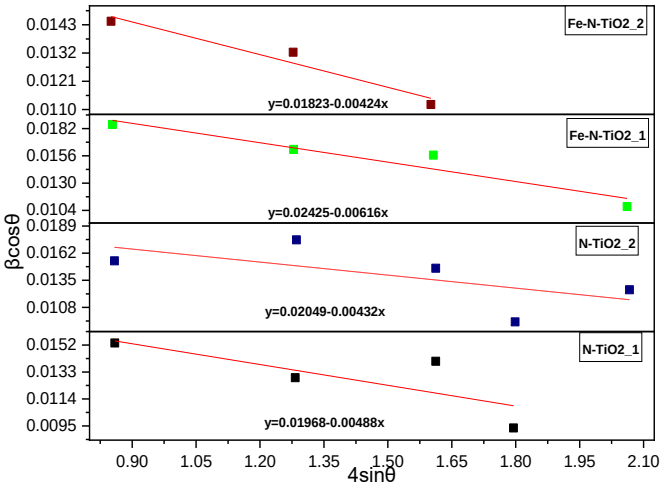

Fig. 3: Williamson and Hall (W-H) plots

However, Williamson & Hall (W-H) plot-method explores broadening of peak by considering weightage to higher diffraction angles than lower and intermediate angles which is not reliable always.

H-W modified equation as shown equation (4) contains the integral breadth, β^*, of the reciprocal lattice point and the lattice planer spacing, d^*, for the reciprocal cell by including lower and intermediate angles which is described by Voigt function as

$$\beta_{hkl}^2 = \beta_L \beta_{hkl} + \beta_G^2 \ldots\ldots\ldots (3)$$

Where, β_L and β_G are Lorentzian and Gaussian components [25]. There by the crystallite size and strain relation given by

$$\left(\frac{\beta_{hkl}^*}{d_{hkl}^*}\right)^2 = \frac{1}{D}\left(\frac{\beta_{hkl}^*}{{d_{hkl}^*}^2}\right) + \left(\frac{\varepsilon}{2}\right)^2 \ldots\ldots\ldots (4)$$

Where,

β^*_{hkl}= $\beta_{hkl} cos\theta/\lambda$ and d^*_{hkl}=2$d_{hkl} sin\theta/\lambda$ by plotting $\left(\frac{\beta^*_{hkl}}{d^*_{hkl}}\right)^2$ vs $\left(\frac{\beta^*_{hkl}}{d^{*2}_{hkl}}\right)$

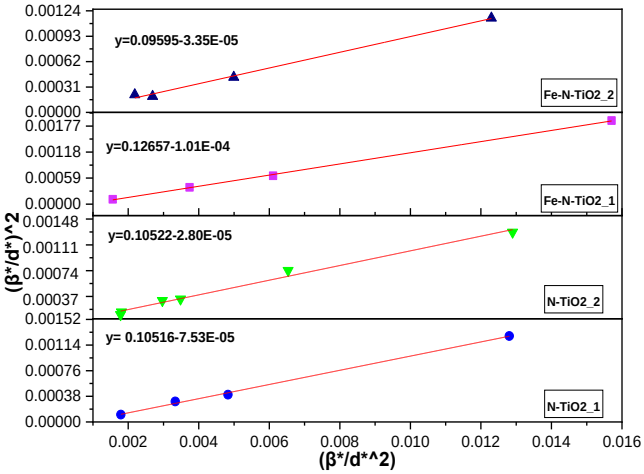

Fig. 4: Halder-Wagner (H-W) plot

The negative sign indicates compressive strain inside the lattice due to replace of higher atomic radii (O^{-2} and Ti^{+4}) with lower one (N^{-3} and Fe^{+3}).

The broad deviation in crystallite size resulted from Debye-Scherer relation & W-H and H-W plots as depicted in Table 4 imply that broadening of FWHM probably prevailing compressive strain in crystal lattice [26]

3.3 Morphology Analysis

Scanning Electron Microscopy (SEM) is used to observe the surface morphology of doped & co-doped Titanium dioxide as shown in Fig.5 (a) to Fig.5(h).

The SEM images explores that the particles in N-TiO_2_1 and N-TiO_2_2 are in spherical shape and agglomerated. Whereas Fe-N-TiO_2_1 is also spherical but more agglomerated than N-TiO_2 samples. But the shape of Fe-N-TiO_2_2 particles has been changed to irregular flakes due to incorporation of high Fe content into TiO_2 crystal lattice. The length of the particles increases drastically from 795.1nm to19µm as well which affects reactive surface area available on the catalyst.

3.4 Optical Analysis

FTIR spectra of doped & co-doped TiO_2 catalysts were carried out in the interval of 500 cm^{-1} - 4000 cm^{-1} wavenumber to identify functional groups as shown in Fig. 6. A broad peak appeared in the range of 3300-3600 cm^{-1}, indicating stretching vibration of O-H group on surface titanium centers of TiO_2, the peak at 2294.12cm^{-1} reveals C-H bonding, vibration of Fe-O bond in between 520-610 cm^{-1}. The Ti-N vibrations in the TiO_2 lattice appeared at the peak in between 1020-1100 cm^{-1} and the O-H bending vibrations of absorbed water molecules were observed at 1620-1640.9 cm^{-1} and further details are summarized in Table 5 related to the position of various peaks.

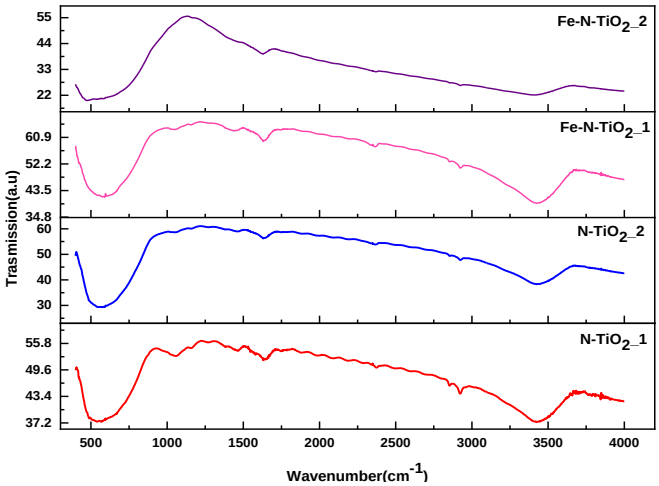

Fig. 6: FTIR Spectra of doped & Co-doped TiO_2 catalysts

3.5 UV–Vis Diffuse Reflectance Spectra

UV-Vis DRS of all four samples are explored and shown in Fig. 7. The band edge is detected when there is a change in concentration Fe, N of doped and co-doped TiO_2, there is a shift of wavelength from a shorter to longer wavelength spectrum (391-535nm) which indicates the Visible region. Co-doping of Fe to N-TiO_2 reflects the increase in absorbance. But much increase in Fe content would inhibit the absorbance [30]. The shift in the wavelength is owing to the charge transfer between the d-electrons of Fe to TiO_2 [31]. Optical energy gap (E_g) of all the synthesized catalysts can be depicted by means of Tauc graphical method as shown in Fig. 8 by using following expression a given by equation (5)[32].

$$\alpha h\nu = A(h\nu - E_g)^{n/2} \ldots\ldots (5)$$

Where, α is the absorption coefficient, hν is the photon energy, n~1 for direct transition between bands and Eg is the band gap energy. From Fig. 8 it's been observed that the optical band gap of modified catalysts decreased from N-TiO_2_1 (3.1eV) to Fe-N-TiO_2_2 (2.8eV). As reported by Alvaro Realpe Jimenez et al., [29] the reduction in band gap is resulted by overlaying of Fe^{3+} (d-orbital) with Ti (d-Orbital) and mixing of the N2p orbital with the O2p orbitals when co-dopant Fe and dopant N are induced into TiO_2 lattice by forming intermediate energy levels which leads to shift of absorption edge towards the visible region [33].

Table-4: Crystallite size and strain by using W-H and H-W plot methods.

S.NO	Catalyst	D (using DS method, nm)	D (using W-H plot method, nm)	Strain(ε_S)	D (using H-W plot method, nm)	Strain(ε)
1	N-TiO_2_1	11.118	7.045	-0.00488	9.51	0.01056
2	N-TiO_2_2	10.133	6.767	-0.00337	9.504	0.02
3	Fe-N-TiO_2_1	9.4357	5.718	-0.00616	7.907	0.01158
4	Fe-N-TiO_2_2	10.392	7.606	-0.00424	10.42	0.01683

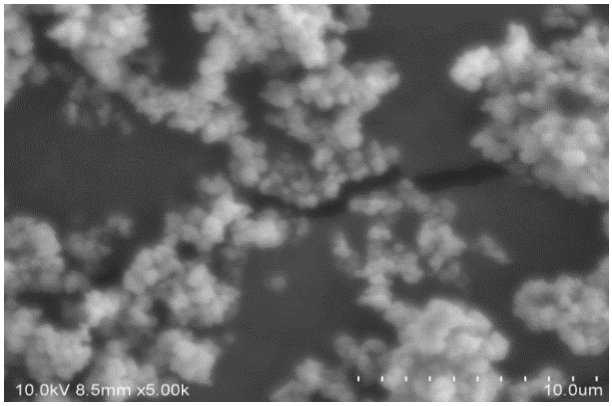

Fig. 5(a):SEM image of N-TiO_2_1

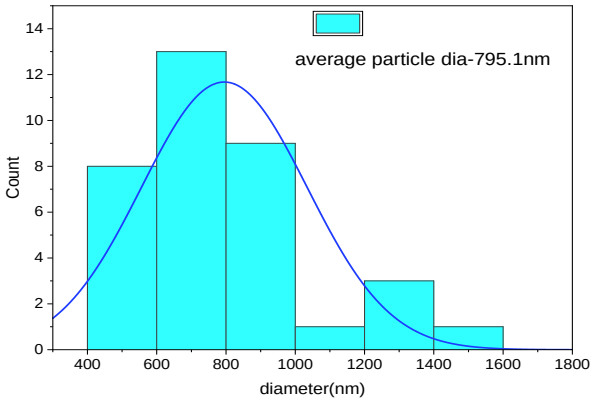

Fig. 5(b): average particle diameter of N-TiO_2_1

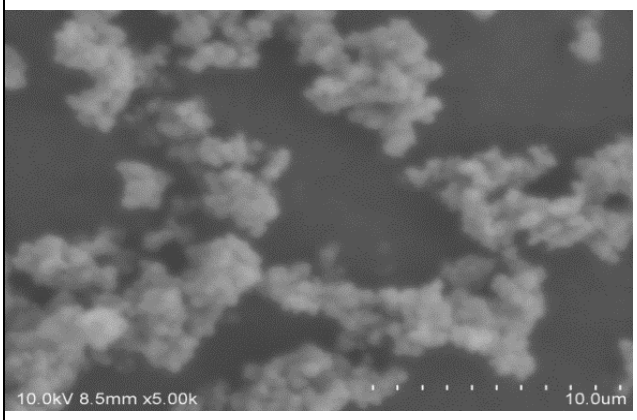

Fig. 5(c):SEM image of N-TiO_2_2

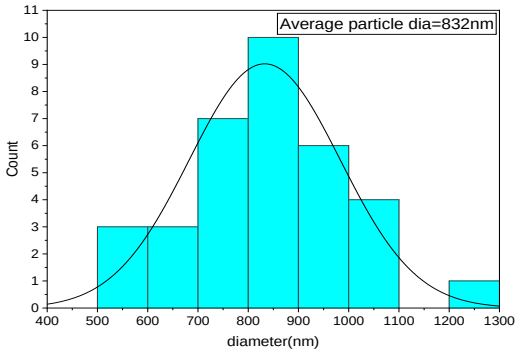

Fig. 5(d): average particle diameter of N-TiO_2_2

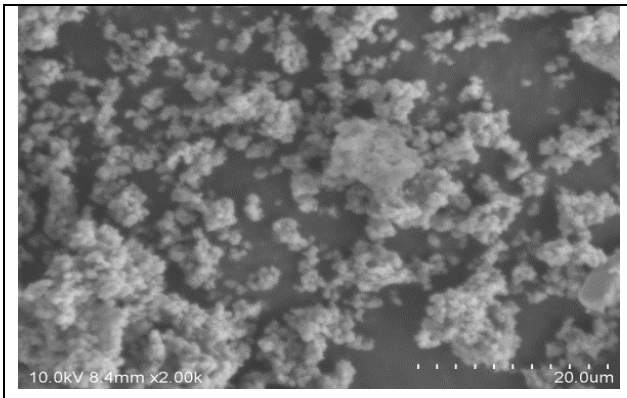

Fig. 5(e):SEM image of Fe- N-TiO_2_1

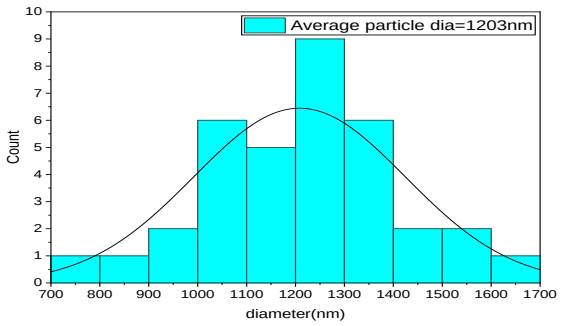

Fig. 5(f): Average particle diameter of Fe- N-TiO_2_1

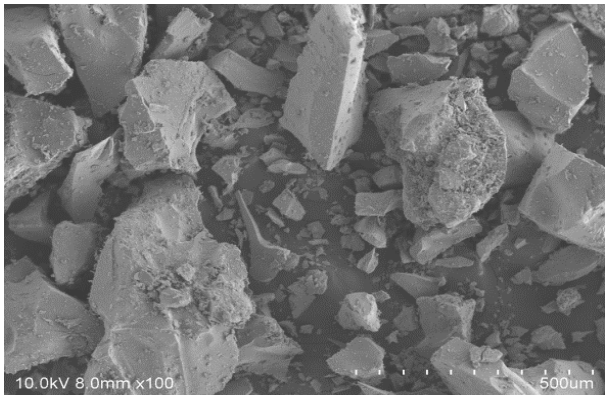

Fig. 5(g):SEM image of Fe-N-TiO_2_2

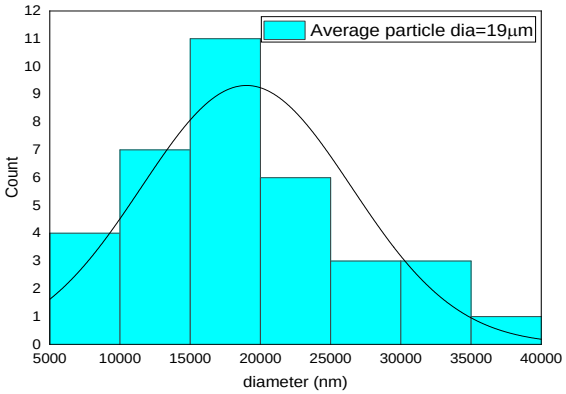

Fig.5(h): Average particle diameter of Fe-N-TiO_2_2

Table-5. Absorption peak positions obtained from FTIR spectra of doped and co-doped TiO_2

Observed absorption peak position (cm^{-1})				Attributed to (reference)
N-TiO_2_1	N-TiO_2_2	Fe-N-TiO_2_1	Fe-N-TiO_2_2	
3419.12	3421.83	3416.05	3398.69	O-H stretching vibrations[26]
2924.18	2924.18	2924.18	2924.18	C-H bonding vibrations [26]
1629.9	1620.9	1629.9	1640.9	O-H bending vibrations [27]
1057	1049.31	1049.31	1174.69	Ti-N bonding vibrations [28]
-	-	574.8	534.3	Fe-O bonding vibrations [29]

At the last, its observed that, co-doping of Iron creates stronger effect compared to doped N-TiO_2 though there is increase in N content from 3 weight % to 6 weight % (where N-TiO_2_1(3.1eV), N-TiO2_2(3.04eV), Fe-N-TiO_2_1 (2.85eV) and Fe-N-TiO_2_2 (2.8eV)) in the reduction of band gap. But much increase in Fe from Fe-N-TiO_2_1 (2.85eV) to Fe-N-TiO_2_2 (2.8eV) content wouldn't lead to an effective narrowing in the energy band gap.

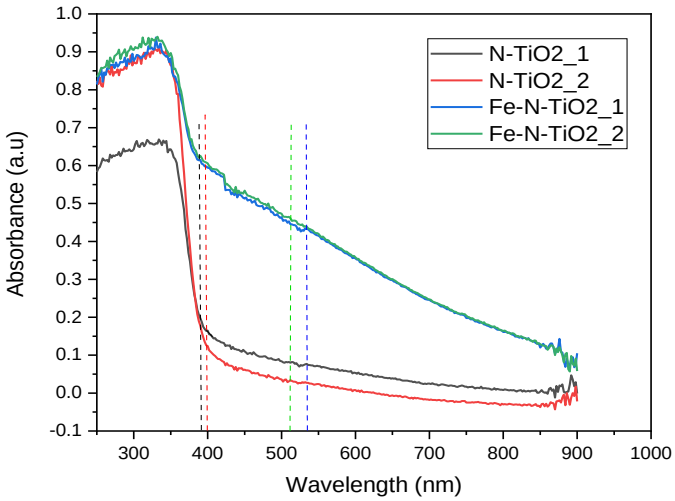

Fig. 7: Diffuse reflectance spectra of all four synthesized catalyst samples

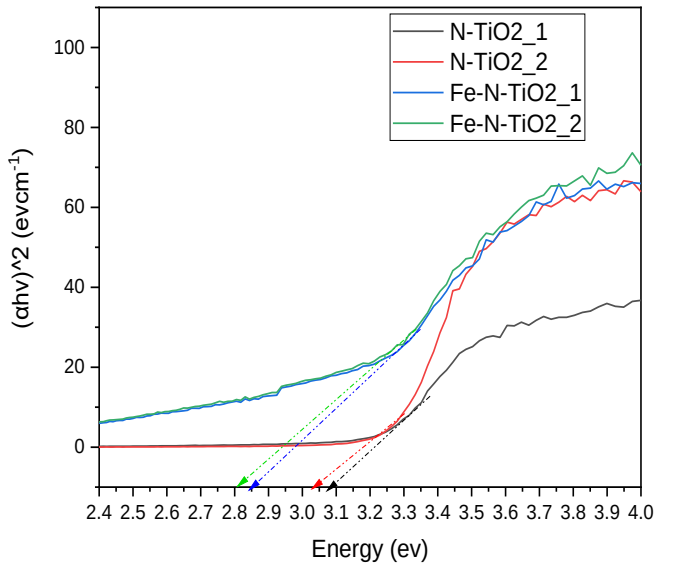

Fig. 8: Tauc graphical plot for the four synthesized catalyst samples

3.6 Selection of Photocatalyst for degradation studies

Among the all modified/ synthesized catalysts Fe-N-TiO_2_1 has been selected for the photo degradation study based on the results obtained through the characterization of all four samples and it's been reported by many researchers [34], the activity of Photocatalyst Fe-N-TiO_2 is more than N-TiO_2 because of reduction in band gap from (3.1 to 2.8eV) and incorporation excessive content of Nitrogen enhances recombination of electron-hole pairs where the oxygen sites are replaced by Nitrogen ions which induces oxygen vacancies [35]. Based on the previous results [22] on doping and co-doping of TiO_2, Co-doping of Fe-N-TiO_2 would be more effective in the degradation of the dye solution. Coming to the results of the characterization of Fe-N-TiO_2_1 and Fe-N-TiO_2_2 the stain in Fe-N-TiO_2_2 is more than Fe-N-TiO_2_1 which may be attributed to lattice dislocations [24] and the band gap is just less than 0.05eV though by increasing the Fe content by double and incorporating the more Fe content inhibiting the absorption edge [30].
Considering all the above, Fe-N-TiO_2_1 was selected as the photocatalyst for the effective degradation of the dye solution.

3.7 Process performance by using Statistical analysis and model development

To optimize the degradation of dye solution RSM study was performed, and results were analyzed by the concept of ANOVA (Analysis of Variance) using Minitab.19.
Table 6. Explores the three-factor CCD quadratic statistical model in coded factors is given below.

$$Y=77.50+5.66X_1+1.23X_2+23.09X_3-2.97X_{12}+11.11X_{22}-27.09X_{32}+2.24X_1X_2+2.06X_1X_3-6.79X_2X_3$$

In this developed model, the positive coefficients responsible for favorable effects on degradation of dye solution for X_1,

Y = - 16.4 + 23.8 catalyst dosage - 0.464 concentration
+ 1.375 reaction time
- 11.9 catalyst dosage*catalyst dosage
+ 0.00549 concentration*concentration
- 0.004816 reaction time*reaction time
+ 0.0993catalyst dosage*concentration
+ 0.0549 catalyst dosage*reaction time
-0.002012 concentration*reaction time

X_2, X_3, X_2^2, X_1X_2 and X_1X_3 ; While the negative coefficients responsible for favorable effects on degradation of dye solution for X_1^2, X_3^2, X_2X_3.The quadratic model in terms of actual factors is given by

3.7.1 Validation of the model

Regression equation modeled were studied for their residual plots as shown in Fig.9(a) and Fig.9(b) representing randomized residual distribution and fitted values within [-7.5, 7.5]. Each plot is drawn against an index of observation order to examine any large deviations which indicates there is no pattern in residual distribution which proves that the residual is independent. Fig. 10 shows the experimental values are close to the center diagonal line, showing the test is significantly in-line with the normal distribution. Post the results of graphical analysis, we have moved towards the numerical analysis using the ANOVA.

Table-6: Three-factor CCD Model Analysis for Observed and Predicted response(Y)

	X_1	X_2	X_3	Y = % Degradation	
Run No.	Catalyst dosage(mg/250ml)	Conc. (mg/l)	Reaction time (min)	Obs.	Pred.
1	0.5	10	30	25.37	26.08
2	1.5	10	30	31	28.80
3	0.5	100	30	39.03	37.60
4	1.5	100	30	52.88	49.31
5	0.5	10	180	78.17	81.72
6	1.5	10	180	91.31	92.69
7	0.5	100	180	63.95	66.13
8	1.5	100	180	86.75	86.03
9	0.5	55	105	73.93	68.87
10	1.5	55	105	75.1	80.19
11	1.0	10	105	90.83	87.38
12	1.0	100	105	86.35	89.83
13	1.0	55	30	20.88	27.31
14	1.0	55	180	79.9	73.50
15	1.0	55	105	76.39	77.50
16	1.0	55	105	76.91	77.50
17	1.0	55	105	77.69	77.50
18	1.0	55	105	77.95	77.50
19	1.0	55	105	78.08	77.50
20	1.0	55	105	78.08	77.50

The above model was statistical validated with significance of 95% confidence interval using ANOVA as shown in Table 7 and factors was resolute using p-values from F- test [22] and R^2. In this model analysis, the terms X_2, X_1^2, $X_1 X_2$ and, $X_1 X_3$ were not significant, indicating variation in these factors may not ominously affect the percentage degradation. R^2 = 0.9781 and the adjusted R^2 = 0.9583 supports our developed model [22].

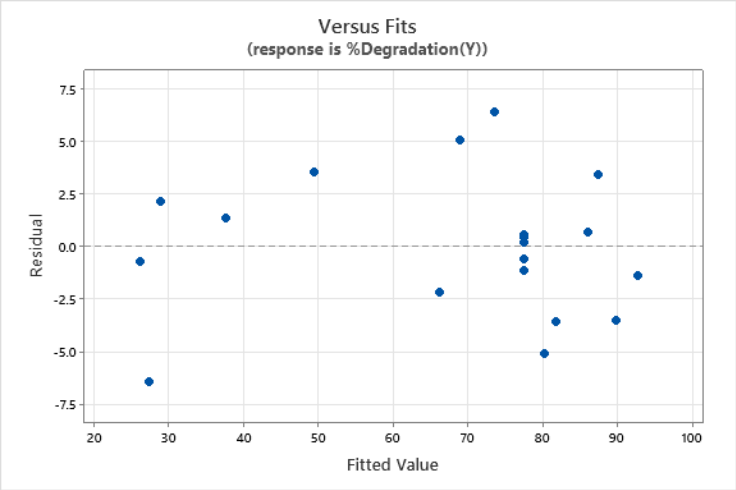

Fig. 9(a): Residual plot for fitted values

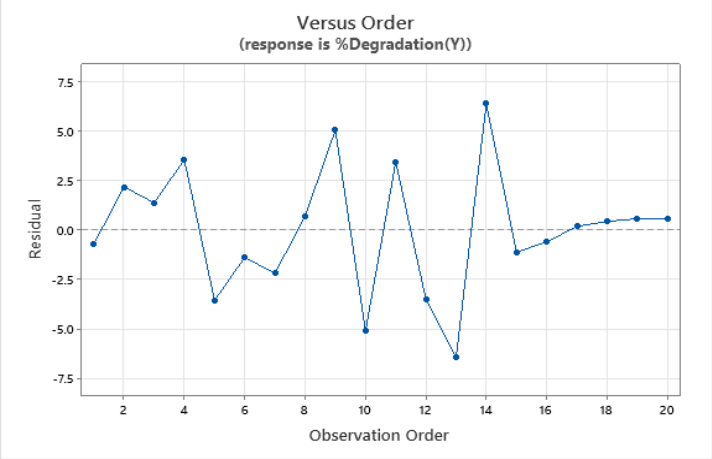

Fig. 9(b): Residual plot for Observation Order

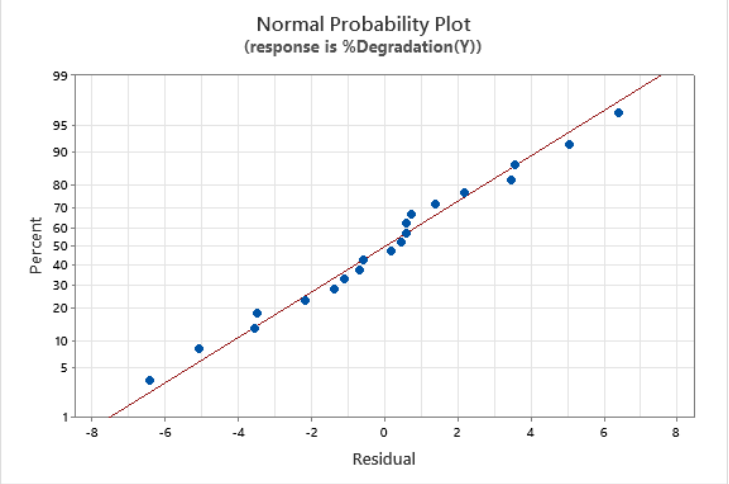

Fig. 10: Normal probability plot

Table-7: Analysis of Variance results for the prediction of response

Source	DF	Adj SS	Adj MS	F-Value	P-Value	Remarks
Model	9	8920.07	991.12	49.52	0.000	Significant
Linear	3	5667.73	1889.24	94.39	0.000	Significant
catalyst dosage (CD)	1	320.24	320.24	16.00	0.003	Significant
Concentration	1	15.08	15.08	0.75	0.406	Not significant
reaction time (RT)	1	5332.40	5332.40	266.41	0.000	Significant
Square	3	2809.68	936.56	46.79	0.000	Significant
CD* CD	1	24.21	24.21	1.21	0.297	Not significant
concentration*concentration	1	339.33	339.33	16.95	0.002	Significant
reaction time*reaction time	1	2018.41	2018.41	100.84	0.000	Significant
2-Way Interaction	3	442.66	147.55	7.37	0.007	Not significant
CD*concentration	1	39.96	39.96	2.00	0.188	Not significant
CD*RT	1	33.87	33.87	1.69	0.223	Not significant
concentration*reaction time	1	368.83	368.83	18.43	0.002	Significant
Error	10	200.16	20.02			
Total	19	9120.23				

We can take the inference from Fig. 11 (a), that the internally studentized residuals vs predicted response confirming the continuous variance assumption [36] and the points were scattered within outlier limits [-2, +2]. Fig. 11(b) shows a minor discrepancy which can be neglected, making the predicted model satisfactory.

3.7.2 Interaction between Model Parameters & 3D Response Surface

3D response surface are plotted as shown in Fig. 12(a), Fig.12(b) and Fig.12(c), showing interaction effects between independent factors for the dye degradation. As per the obtained results from the fitted model as shown in Table 7, among all the factors, the interaction between catalyst dosage, concentration (X_1X_2) and catalyst dosage, reaction time (X_2X_3) were showing non- significant terms which has least effects on degradation of dye solution. Whereas interaction between concentrations, reaction time (X_2X_3) shown a significant effect on system response. Based on the above, we can deduce the optimized values for the interaction effect, which are shown in the Fig. 13.

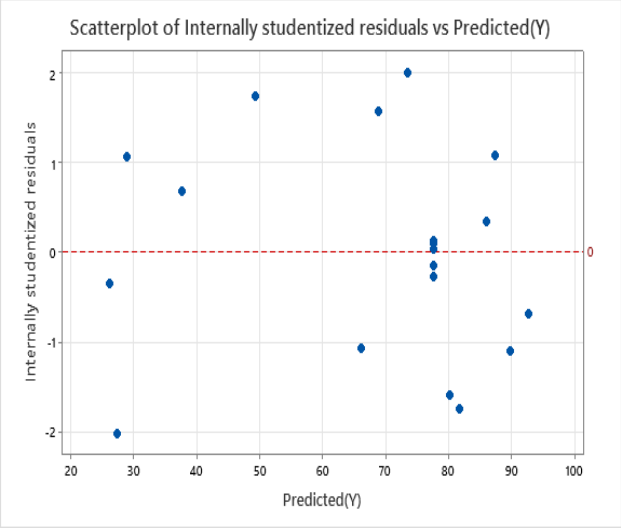

Fig.11 (a): Scattered plot of internally studentized residuals vs Predicted(Y)

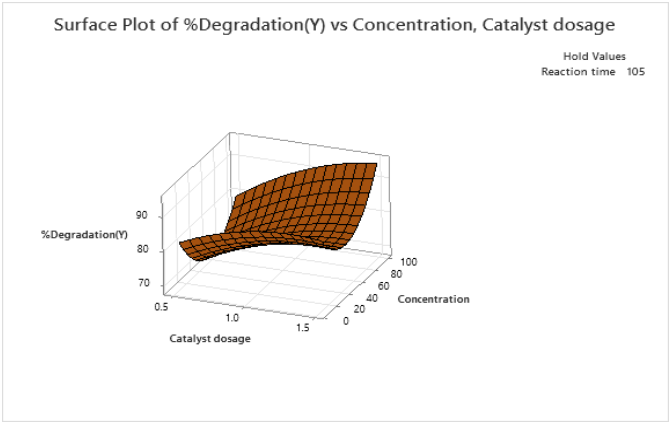

Fig. 12(a): Surface plot of % Degradation vs Concentration (mg/l) and Catalyst dosage (g)

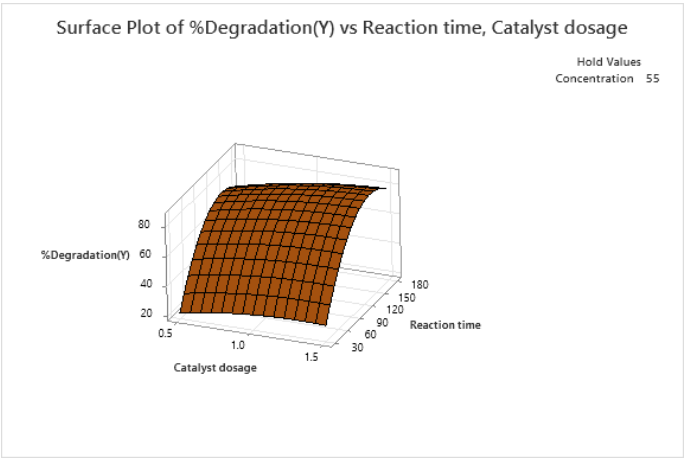

Fig. 12(b): Surface plot of % Degradation Vs Catalyst dosage (g) and Reaction time (min)

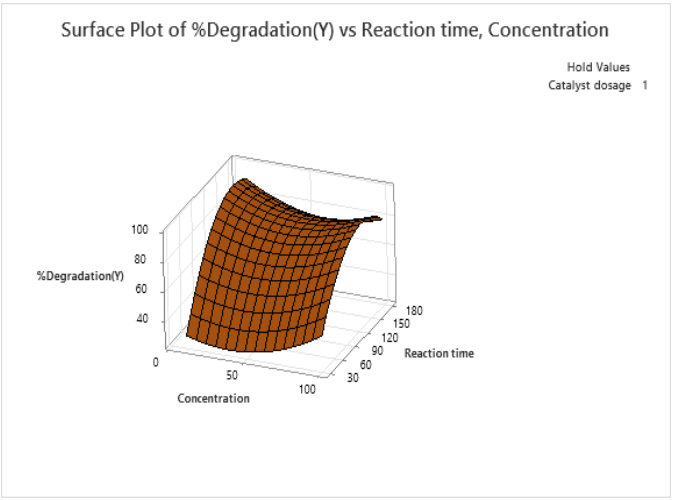

Fig. 12 (c): Surface plot of % Degradation Vs Concentration (mg/l) and Reaction time (min)

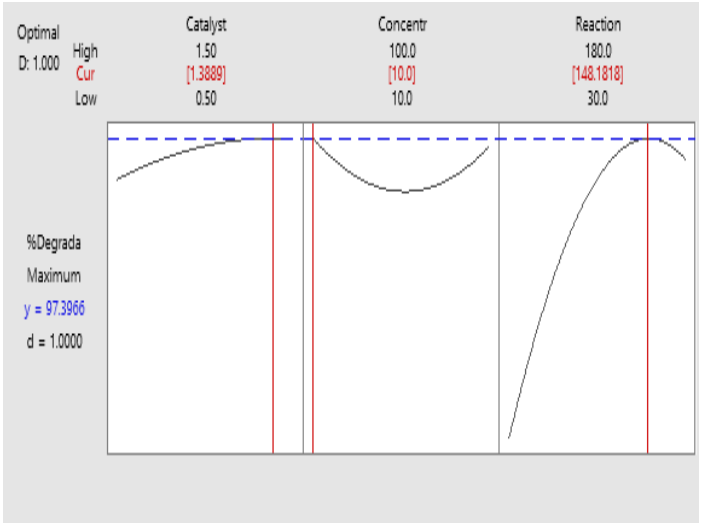

Fig. 13: Optimization plots for the observed model

4. OPTIMIZATION OF THE PROCESS PARAMETERS & KINETIC STUDIES

RSM Analysis was used to predict maximum percentage of degradation of dye solution under optimized experimental settings for the following factors: Catalyst dosage (X_1), Concentration (X_2), and reaction time (X_3). These parameters were optimized by using central composite design method as a part of design of experiments in the statistical software Minitab-19 built in method. The desirability value was aimed at 1 while acquiring a percentage degradation of 97.39% under optimum conditions of the catalyst dosage of 1.388 g/250 ml concentration of 10 ppm with a reaction time of 148 minutes. At the end, by conducting an extra set of experiments the optimum observed conditions of catalyst dosage of 1.388 g/250 ml concentration of 10 ppm with a reaction time of 148 minutes achieved 96.2% degradation which indicates the validation of the predicted model.

The photocatalytic first order reaction rate constant of the %degradation was determines from the Fig. 14 by plotting $ln\frac{A_o}{A}$ vs reaction time (t) and the first-order rate constant and the coefficient of determination (R^2) were 0.0158min^{-1} and 0.952 were determined.

5. CONCLUSIONS

Structural and optical properties of TiO_2 altered with the addition of metal (Fe) and non-metal (N) by using Co-doping mechanism was shown good results in successful employment of solar radiation for the degradation of textile dye RO86. The Characterization techniques explored the enough information on selection of catalyst by varying the composition of N and Fe with respect to the TiO_2. This study applied Response Surface Methodology combined with 3

factors CCD to model the system performance that is % degradation of RO86 dye as target response. The degradation efficiency of 97.39% achieved under optimized conditions of the catalyst dosage of 1.388 g/250 ml, concentration of 10 ppm with a reaction time of 148 minutes. The study of kinetics has given photocatalytic first order reaction rate constant which could be utilized as a future reference on photoreactor design and scale-up studies.

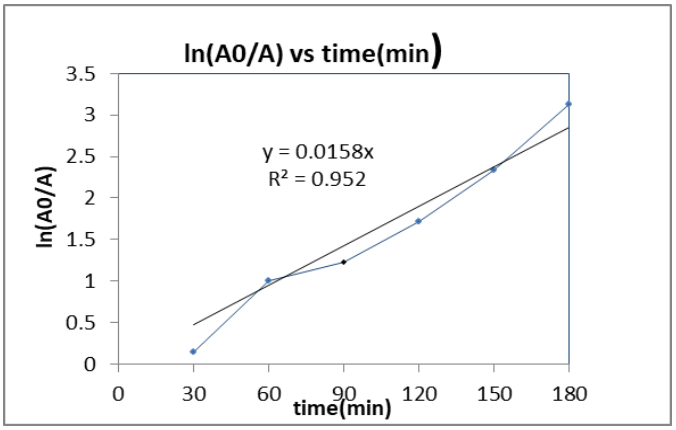

Fig.14: photo catalytic treatment of RO86 under optimum conditions

ACKNOWLEDGEMENT

This paper is based upon work supported by University College of Technology OUCT, OU, Hyderabad and Department of Chemical Engineering & Civil Engineering at Rajiv Gandhi University of Knowledge Technology (RGUKT) Basar.

REFERENCES

[1] A. Giwa, P. O. Nkeonye, K. A. Bello, E. G. Kolawole, and A. O. Campos, "Solar photocatalytic degradation of reactive yellow 81 and reactive violet 1 in aqueous solution containing semiconductor oxides," *Int. J. Appl.*, vol. 2, no. 4, pp. 90–105, 2012.

[2] P. C. C. Faria, J. J. M. Orfao, and M. F. R. Pereira, "Adsorption of anionic and cationic dyes on activated carbons with different surface chemistries," *Water Res.*, vol. 38, no. 8, pp. 2043–2052, 2004.

[3] K. Venkataraman, *The Chemistry of Synthetic Dyes V4*, vol. 4. Elsevier, 2012.

[4] M. A. Brown and S. C. De Vito, "Predicting azo dye toxicity," *Crit. Rev. Environ. Sci. Technol.*, vol. 23, no. 3, pp. 249–324, 1993.

[5] A. A. Murgod, M. S. Golangade, P. B. Koli, B. Samyak, and N. M. Naik, "Photo-Oxidation Process–Application for Removal of Color from Textile Industry Effluent," *Res. J. Chem. Sci. ISSN*, vol. 2231, p. 606X, 2012.

[6] R. G. Saratale, G. D. Saratale, J.-S. Chang, and S. P. Govindwar, "Bacterial decolorization and degradation of azo dyes: a review," *J. Taiwan Inst. Chem. Eng.*, vol. 42, no. 1, pp. 138–157, 2011.

[7] V. D. Gosavi and S. Sharma, "A general review on various treatment methods for textile wastewater," *J. Environ. Sci. Comput. Sci. Eng. Technol.*, vol. 3, no. 1, pp. 29–39, 2014.

[8] A. El Mragui, Y. Logvina, L. Pinto da Silva, O. Zegaoui, and J. C. G. Esteves da Silva, "Synthesis of Fe-and Co-doped TiO2 with improved photocatalytic activity under visible irradiation toward carbamazepine degradation," *Materials (Basel).*, vol. 12, no. 23, p. 3874, 2019.

[9] A. Carabin, P. Drogui, and D. Robert, "Photo-degradation of carbamazepine using TiO2 suspended photocatalysts," *J. Taiwan Inst. Chem. Eng.*, vol. 54, pp. 109–117, 2015.

[10] L. Pirinejad, A. Maleki, B. Shahmoradi, H. Daraei, J.-K. Yang, and S.-M. Lee, "Synthesis and application of Fe-N-Cr-TiO2 nanocatalyst for photocatalytic degradation of Acid Black 1 under LED light irradiation," *J. Mol. Liq.*, vol. 279, pp. 232–240, 2019.

[11] S. G. Ghugal, S. S. Umare, and R. Sasikala, "Enhanced photocatalytic activity of TiO2 assisted by Nb, N and S multidopants," *Mater. Res. Bull.*, vol. 61, pp. 298–305, 2015.

[12] M. Tahir and N. S. Amin, "Advances in visible light responsive titanium oxide-based photocatalysts for CO2 conversion to hydrocarbon fuels," *Energy Convers. Manag.*, vol. 76, pp. 194–214, 2013.

[13] F. Tian, Z. Wu, Y. Tong, Z. Wu, and G. Cravotto, "Microwave-assisted synthesis of carbon-based (N, Fe)-codoped TiO 2 for the photocatalytic degradation of formaldehyde," *Nanoscale Res. Lett.*, vol. 10, pp. 1–12, 2015.

[14] B. Wawrzyniak, A. W. Morawski, and B. Tryba, "Preparation of TiO2-nitrogen-doped photocatalyst active under visible light," *Int. J. Photoenergy*, vol. 2006, 2006.

[15] H.-H. Cheng, S.-S. Chen, S.-Y. Yang, H.-M. Liu, and K.-S. Lin, "Sol-Gel hydrothermal synthesis and visible light photocatalytic degradation performance of Fe/N

codoped TiO2 catalysts," *Materials (Basel).*, vol. 11, no. 6, p. 939, 2018.

[16] X. Cao, C. Liu, Y. Hu, W. Yang, and J. Chen, "Synthesis of N/Fe comodified TiO2 loaded on bentonite for enhanced photocatalytic activity under UV-Vis light," *J. Nanomater.*, vol. 2016, p. 1, 2016.

[17] A. Sadeghzadeh-Attar, "Photocatalytic degradation evaluation of N-Fe codoped aligned TiO 2 nanorods based on the effect of annealing temperature," *J. Adv. Ceram.*, vol. 9, pp. 107–122, 2020.

[18] S. Ahmadi, L. Mohammadi, C. A. Igwegbe, S. Rahdar, and A. M. Banach, "Application of response surface methodology in the degradation of Reactive Blue 19 using H 2 O 2/MgO nanoparticles advanced oxidation process," *Int. J. Ind. Chem.*, vol. 9, pp. 241–253, 2018.

[19] C. Thambiliyagodage and L. Usgodaarachchi, "Photocatalytic activity of N, Fe and Cu co-doped TiO2 nanoparticles under sunlight," *Curr. Res. Green Sustain. Chem.*, vol. 4, p. 100186, 2021.

[20] M. Zulfiqar, M. F. R. Samsudin, and S. Sufian, "Modelling and optimization of photocatalytic degradation of phenol via TiO2 nanoparticles: An insight into response surface methodology and artificial neural network," *J. Photochem. Photobiol. A Chem.*, vol. 384, p. 112039, 2019.

[21] J.-K. Park, G.-M. Lee, C.-Y. Lee, K.-B. Hur, and N.-H. Lee, "Analysis of siloxane adsorption characteristics using response surface methodology," *Environ. Eng. Res.*, vol. 17, no. 2, pp. 117–122, 2012.

[22] Y. P. Lin and M. Mehrvar, "Photocatalytic treatment of an actual confectionery wastewater using Ag/TiO2/Fe2O3: optimization of photocatalytic reactions using surface response methodology," *Catalysts*, vol. 8, no. 10, p. 409, 2018.

[23] T. B. Nguyen, J. P. Deloume, and V. Perrichon, "Study of the redox behaviour of high surface area CeO2–SnO2 solid solutions," *Appl. Catal. A Gen.*, vol. 249, no. 2, pp. 273–284, 2003.

[24] D. Nath, F. Singh, and R. Das, "X-ray diffraction analysis by Williamson-Hall, Halder-Wagner and size-strain plot methods of CdSe nanoparticles-a comparative study," *Mater. Chem. Phys.*, vol. 239, p. 122021, 2020.

[25] L. Motevalizadeh, Z. Heidary, and M. E. Abrishami, "Facile template-free hydrothermal synthesis and microstrain measurement of ZnO nanorods," *Bull. Mater. Sci.*, vol. 37, pp. 397–405, 2014.

[26] A. Srivastava, N. Kumar, and S. Khare, "Enhancement in UV emission and band gap by Fe doping in ZnO thin films," *Opto-Electronics Rev.*, vol. 22, pp. 68–76, 2014.

[27] I. Ganesh *et al.*, "Preparation and characterization of Fe-doped TiO 2 powders for solar light response and photocatalytic applications," *Process. Appl. Ceram.*, vol. 6, no. 1, pp. 21–36, 2012.

[28] A. Realpe Jimenez, D. Nunez, N. Rojas, Y. Ramirez, and M. Acevedo, "Effect of Fe–N codoping on the optical properties of TiO2 for use in photoelectrolysis of water," *ACS omega*, vol. 6, no. 7, pp. 4932–4938, 2021.

[29] F. Malega, I. P. T. Indrayana, and E. Suharyadi, "Synthesis and characterization of the microstructure and functional group bond of fe3o4 nanoparticles from natural iron sand in Tobelo North Halmahera," *J. Ilm. Pendidik. Fis. Al-Biruni*, vol. 7, no. 2, pp. 13–22, 2018.

[30] J. Song *et al.*, "Preparation, characterization, and photocatalytic activity evaluation of Fe–N-codoped TiO 2/fly ash cenospheres floating photocatalyst," *Environ. Sci. Pollut. Res.*, vol. 23, pp. 22793–22802, 2016.

[31] Y. Yalçın, M. Kılıç, and Z. Çınar, "Fe+ 3-doped TiO2: A combined experimental and computational approach to the evaluation of visible light activity," *Appl. Catal. B Environ.*, vol. 99, no. 3–4, pp. 469–477, 2010.

[32] S. D. Delekar, H. M. Yadav, S. N. Achary, S. S. Meena, and S. H. Pawar, "Structural refinement and photocatalytic activity of Fe-doped anatase TiO2 nanoparticles," *Appl. Surf. Sci.*, vol. 263, pp. 536–545, 2012.

[33] D. Nassoko, Y.-F. Li, H. Wang, J.-L. Li, Y.-Z. Li, and Y. Yu, "Nitrogen-doped TiO2 nanoparticles by using EDTA as nitrogen source and soft template: Simple preparation, mesoporous structure, and photocatalytic activity under visible light," *J. Alloys Compd.*, vol. 540, pp. 228–235, 2012.

[34] A. Mancuso, O. Sacco, D. Sannino, S. Pragliola, and V. Vaiano, "Enhanced visible-light-driven photodegradation of Acid Orange 7 azo dye in aqueous solution using Fe-N co-doped TiO2," *Arab. J. Chem.*, vol. 13, no. 11, pp. 8347–8360, 2020.

[35] C. Di Valentin, G. Pacchioni, and A. Selloni, "Origin of the different photoactivity of N-doped anatase and rutile TiO 2," *Phys. Rev. B*, vol. 70, no. 8, p. 85116, 2004.

[36] C. F. Bustillo-Lecompte and M. Mehrvar, "Treatment of an actual slaughterhouse wastewater by integration of biological and advanced oxidation processes: Modeling, optimization, and cost-effectiveness analysis," *J. Environ. Manage.*, vol. 182, pp. 651–666, 2016.